Title
Bifurcation analysis of an agent-based model for predator–prey interactions

Journal
Ecological Modelling, 317(C)

ISSN
0304-3800

Authors
Colon, C
Claessen, D
Ghil, M

Publication Date
2015-12-01

DOI
10.1016/j.ecolmodel.2015.09.004

Peer reviewed

Bifurcation analysis of an agent-based model for predator–prey interactions

C. Colon[a,b,d,*], D. Claessen[b,c], M. Ghil[a,b,e]

[a] *Laboratoire de Meteorologie Dynamique, Ecole Normale Supérieure, F-75230 Paris Cedex 05, France*
[b] *Environmental Research and Teaching Institute, Ecole Normale Supérieure, F-75230 Paris Cedex 05, France*
[c] *Institut de Biologie de l'Ecole Normale Supérieure (CNRS UMR 8197, INSERM U1024), Ecole Normale Supérieure, 46 rue d'Ulm, 75005 Paris, France*
[d] *Applied Mathematics Department, Ecole Polytechnique, Route de Saclay, 91128 Palaiseau, France*
[e] *Department of Atmospheric and Oceanic Sciences, University of California at Los Angeles, Los Angeles, CA 90095-1565, USA*

Abstract

The Rosenzweig-MacArthur model is a set of ordinary differential equations (ODEs) that provides an aggregate description of the dynamics of a predator–prey system. When including an Allee effect on the prey, this model exhibits bistability and contains a pitchfork bifurcation, a Hopf bifurcation and a heteroclinic bifurcation. We develop an agent-based model (ABM) on a two-dimensional, square lattice that encompasses the key assumptions of the aggregate model. Although the two modelling approaches – ODE and ABM – differ, both models exhibit similar bifurcation patterns. The ABM model's behaviour is richer and it is analysed using advanced statistical methods. In particular, singular spectrum analysis is used to robustly locate the transition between apparently random, small-amplitude fluctuations around a fixed point and stable, large-amplitude oscillations. Critical slowing down of model trajectories anticipates the heteroclinic bifurcation. Systematic comparison between the ABM and the ODE models' behaviour helps one understand the predator–prey system better; it provides guidance in model exploration and allows one to draw more robust conclusions on the nature of predator–prey interactions.

Keywords:
ODE, Hopf bifurcation, heteroclinic bifurcation, time series analysis, singular spectrum analysis, critical transition, early-warning signals

1. Introduction and motivation

Ecologists are more and more frequently asked to make predictions about the potential effects of specific changes to an ecosystem or a community of species. This demand is particularly vivid in the context of climate change (Lavergne et al., 2010; Valladares et al., 2014) or resource management. It especially applies when anthropic harvesting is at play, as in fisheries (Lindegren et al., 2010), or when biological factors might disturb an established community of species, as in cases of non-endemic species invading an ecosystem (Crowl et al., 2008). Understanding

*Corresponding author
Email address: celian.colon@polytechnique.edu (C. Colon)

these consequences is also relevant when the driver of changes is internal, in particular through evolutionary processes (Ferrière, 2009).

Whether the engine of change is external or internal, analysing the consequences requires a comprehensive understanding of the community dynamics. Achieving such an understanding has proven to be a challenging task. Observational and experimental data show that an ecological system composed of only two interacting species can exhibit non-trivial dynamics, such as bistability and oscillations (e.g., Fussmann et al., 2000). The importance of non-linear mechanisms in leading to such dynamics has motivated theoretical work on simple models to characterise the dynamical regimes, identify and circumscribe basins of attraction, and locate bifurcations or regime shifts. To do so, ecologists have borrowed mathematical concepts and tools from other disciplines and tried a variety of modelling techniques, especially using systems of ordinary differential equations (ODEs).

A recent innovation is the development of agent-based models (ABMs), also called individual-based models in the ecological literature. ABMs simulate systems described by the rules of interaction among autonomous individuals. According to DeAngelis and Mooij (2005), some scholars view ABMs as exploratory tools that extend classical aggregate models, whereas others suggest that ABMs provide a methodological basis on which to build a novel research paradigm (Grimm et al., 1999; Grimm and Railsback, 2005). In the field of population dynamics, ABMs have helped investigate the role of local interactions (Mccauley et al., 1993) and spatial dynamics (Dieckmann et al., 2000); they are also being increasingly employed to study evolutionary dynamics (Łomnicki, 1999; Gras et al., 2009).

Can ABMs help the understanding of community dynamics? How can their use complement the classic ODE approach? In climate sciences, it has been proposed to advance knowledge by moving across a hierarchy of models of the same class of phenomena (Schneider and Dickinson, 1974; Ghil, 2001; Dijkstra and Ghil, 2005). This hierarchy ranges from low-resolution 'toy' models, which help understand the general behaviour of the system, all the way to very detailed 'realistic' models, which may be used for real-time forecasting of weather or climate. Moving up the hierarchy implies adding mechanisms and improving resolution, which often comes at the cost of losing analytical tractability and insight. Detailed models have to be integrated numerically, and analysing their outputs may require complex statistical manipulations. Going back and forth between different levels allows one to test the robustness of the conclusions and guide fruitful improvements of the models at each level of the hierarchy.

The hierarchical modelling approach could be insightfully applied to study the dynamics of communities and even ecosystems. It would thus appear that classical ODE systems, such as the Lotka-Voltera equations, are toy models — in the hierarchical modelling terminology (Ghil, 2001) — whereas the ABM framework is more appropriate for developing detailed models. ABMs can be seen as more realistic, since agents often correspond to observable organisms (Bonabeau, 2002). Contrasting the results of different models has already allowed ecologists to point out some mechanisms that a single-model approach may overlook, such as the influence of spatial distribution and localized interactions (Donalson and Nisbet, 1999; Durrett and Levin, 1994), of physiological structure (De Roos and Persson, 2005) and of heterogeneity (Hastings, 1990). In particular, Dieckmann et al. (2000) pointed out instances in which the dynamics of mean-field models differ from the ABMs they derive from, and proposed new mathematical methods to

integrate the spatially distributed aspects of ABMs into ODEs, such as moment methods (Law and Dieckmann, 2000) or pair-wise approximations (van Baalen, 2000).

In this paper, we illustrate the hierarchical modelling approach by revisiting a classical predator–prey system and comparing the dynamical behaviour of an ABM with that of an ODE model. The guiding thread of this comparison is to determine whether the two models' bifurcation patterns — which summarise the key features of a system's dynamics — are qualitatively similar, even though each model is built upon distinct and complementary principles.

The key components of ODE models are the macro-level feedback mechanisms. Individuals, as distinct entities, do not play any role per se. The dynamics results from the relative abundance of each population, expressed through the principle of 'mass-action'. In ABMs, the system-level dynamics results from the micro-level actions of autonomous individuals. They follow rules, but their effective actions depend on local contingencies. In addition, agents may have only limited information on the system they are embedded in. Grimm and Railsback (2005) argue that reproducing results of a classical ODE model with ABMs often led to the design of models that are incomplete, not robust, and therefore lacking in interest.

In this paper, we do not aim to reproduce the outputs of an ODE model with an ABM, neither do we want to perform any quantitative comparison. Our objective is to establish whether the behaviour patterns of the two models are in qualitative agreement, i.e., whether the solution types — bistable, oscillatory and irregular — are in one-to-one correspondence, including the transitions between these regimes of behaviour, as long as the two models, while conceptually different, rely on the same key assumptions about the system under scrutiny. In addition, we are interested to find out — provided there is a good correspondence in regime types and bifurcations between the aggregate ODE model and the ABM — whether ideas on early warning that were developed for ODE models Scheffer et al. (2009) can help formulate such early warnings for ABMs.

The qualitative comparison between our ODE model and the ABM is carried out by computing the corresponding bifurcation diagrams of the two models. To do this, we need to locate the bifurcation points in our ABM. The identification of attractors has not been the main emphasis of ecological ABM studies, which tend to focus instead on the emergence of spatial patterns (Grimm and Railsback, 2005; Railsback and Grimm, 2011). Analysing attractor types and the transitions between them as significant model parameters change — i.e., studying the models' bifurcations — is quite helpful in understanding regime shifts. These shifts are crucial ecological phenomena and applying bifurcation-theoretical methods to ABM studies thus follows the call of Scholl (2001) to tighten connections between agent-based modelling and dynamical systems theory. In particular, we propose and apply a method to detect the transition between regular oscillations and irregular fluctuations around a steady state.

In section 2.1, we present the behaviour of a classical ODE model of predator–prey systems: the Rosenzweig-McArthur model with strong Allee effect on the prey. In section 2.2, we formulate an ABM in which the key mechanisms that enter the aggregate model emerge spontaneously; these mechanisms include the functional response and the Allee effect. We then define, in section 2.4, the experimental protocol of the simulations and explain the methods we use to analyse the resulting ABM model.

In section 3, we present the results and compare the bifurcation diagrams obtained for the two models, while focussing on the Hopf bifurcation in section 3.2 and on the heteroclinic one in section 3.3. In section 4, we explore early-warning signals for the global transitions and test them when endogenous processes or exogenous forcing modify slowly the model parameters. Finally, we discuss the methodological implications of our work within ABM studies.

2. Models and methodology

2.1. The aggregate model and its behaviour

We study the Rosenzweig-McArthur model with strong Allee effect on the prey. Boukal et al. (2007) analysed how the 'route to collapse' featured in Rosenzweig-McArthur models is influenced by the addition of either a weak or a strong Allee effect, and by the sigmoidicity of the functional response. The system's collapse occurs through a global bifurcation, characterised by an heteroclinic orbit (van Voorn et al., 2007). Wang et al. (2011) performed a rigorous analysis of the model, and focussed on the existence and uniqueness of limit cycles after the Hopf bifurcation. González-Olivares et al. (2006) performed a similar analysis with an Holling type III functional response.

Let X denote the prey population and Y the predator population. The dynamics is governed by the following two coupled ODEs:

$$\frac{\mathrm{d}X}{\mathrm{d}t} = rX(1-\frac{X}{K})(X-A) - \alpha\frac{X}{X+S}Y\,, \tag{1a}$$

$$\frac{\mathrm{d}Y}{\mathrm{d}t} = \rho\alpha\frac{X}{X+S}Y - dY\,. \tag{1b}$$

This model has seven parameters, whose definitions and values are listed in Table 1. We will also use $\mathbf{Z}(t) = (X(t), Y(t))$ to denote the state of our two-species ecosystem as a function of time t.

Table 1: Summary of the parameters used in the ODE model

Parameter	Definition	Value
r	Prey's maximal growth rate	1
K	Prey's carrying capacity	1
A	Prey's Allee effect threshold	0.1
α	Predator's attack rate	1
S	Predator's half saturation constant	0.4
ρ	Predators' conversion rate	$0 \leq \rho \leq 1$
d	Predator's death rate	0.4

The model's dynamics can be summarised in a two-dimensional regime diagram usually plotted in the (d, A)-plane; see, for instance, González-Olivares et al. (2006); Boukal et al. (2007) and van Voorn et al. (2007). We choose

ρ instead of d, which leads to a very similar diagram, plotted here as Fig. 1. The regime boundaries between regions (1) and (2) and between regions (2) and (3) were obtained analytically. The location of the boundary between regions (3) and (4) was identified numerically, using continuation methods (Dhooge et al., 2003) to track the growth and collapse of the limit cycle.

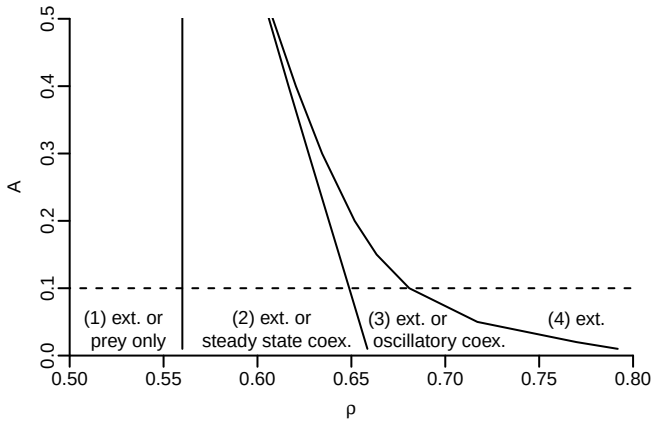

Figure 1: Regime diagram of the aggregate model. The dashed line corresponds to the section along which the bifurcation diagram in Fig. 3 is calculated. 'Ext.' stands for extinction, 'coex.' for coexistence.

In region (4) of the figure, there is only one attractor, which is a fixed point, and all orbits converge to the origin. Predators overexploit prey, whose density sinks below the Allee effect threshold. The prey go extinct, followed by the predators.

In the three other regions, the system is bistable: the state diagrams (not shown) exhibit two basins of attraction whose common boundary is a smooth separatrix, cf. Fig. 2a below. In the portion of the phase plane located above the separatrix — i.e., at more abundant predator population — the system behaves as in region (4).

To understand better the dynamics below the separatrix in Fig. 2a, we calculated the bifurcation diagram shown in Fig. 3 with respect to the parameter ρ, at $A = 0.1$ (dashed line in Fig. 1).

Four types of behaviour are observed:

- *Prey-only*: for $\rho < 0.56$, $(X = K \neq 0, Y = 0)$ is an attractor. The predators are not efficient enough and go extinct; the prey, freed from predation, fill the carrying capacity; see region (1) of Fig. 1.

- *Steady-state coexistence*: when ρ exceeds 0.56, the non-trivial steady state $(X = K, Y = 0)$ changes from being a stable node, or sink, to being a saddle, and a new attracting fixed point P_S emerges: the two populations coexist at steady densities; see region (2) in the figure.

- *Oscillatory coexistence*: at $\rho = 0.65$, the new, stable fixed point undergoes a Hopf bifurcation and an attracting limit cycle emerges. The two populations coexist with periodic densities; see region (3).

- *Extinction*: as ρ increases further, the period and amplitude of the oscillations continue to increase until the limit cycle merges with the separatrix and becomes an heteroclinic orbit linking the two saddle points $(K, 0)$ and $(A, 0)$. This global bifurcation provokes the collapse of the bistability, and the system reaches region (4); see Fig. 2b.

To understand the nature of the bifurcation at $\rho = 0.56$, denoted by 'BP' in Fig. 3, requires a second look at the ODE system (1). In fact, the predator equation (1b) is invariant under a change of Y into $-Y$. While negative populations are not realistic, this mirror symmetry implies that BP is a pitchfork bifurcation, with transfer of stability from the prey-only fixed point $(K, 0)$ to the new stable fixed point with non-zero predator population, $Y \neq 0$.

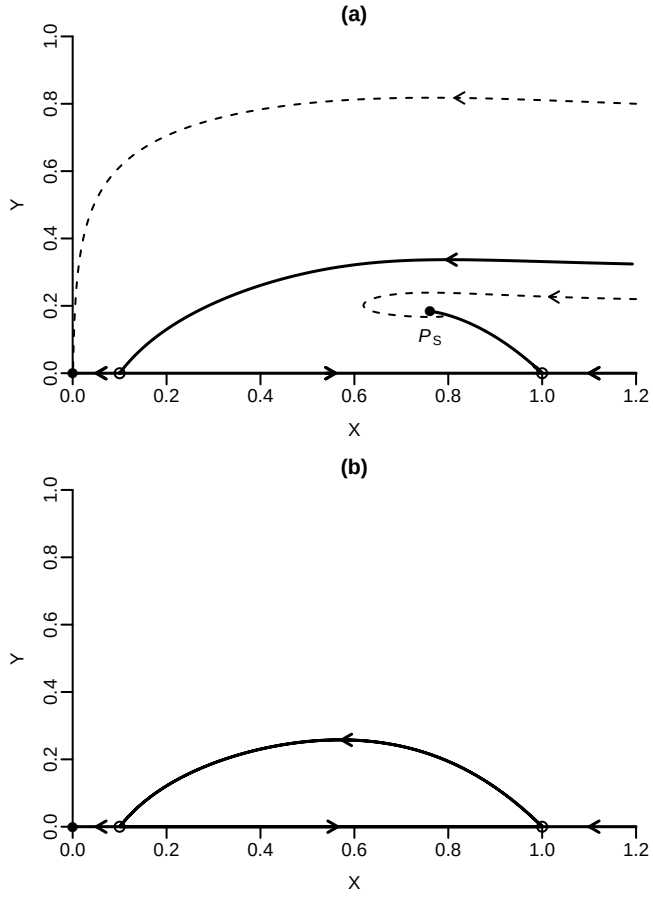

Figure 2: Phase plane of the aggregate model with (a) $\rho = 0.61$ and (b) $\rho = 0.6808$. The solid curves correspond to the invariant manifolds of the saddle points $(A, 0)$ and $(K, 0)$, indicated by open circles. In panel (a), the stable manifold of $(A, 0)$ is a separatrix that forms the mutual boundary of two regions. In either one of the two regions, all the trajectories — illustrated by one dashed curve in either region — converge to a fixed point, namely the origin and P_S, respectively; the latter two are indicated by a filled circle each. In panel (b), the unstable manifold of $(K, 0)$ coincides with the stable manifold of $(A, 0)$, thus forming a heteroclinic connection between the two saddles.

2.2. ABM model formulation

The model description follows the Overview, Design concepts, Details (ODD) protocol of Grimm et al. (2006, 2010).

Purpose

The purpose of the model is to understand how the dynamics of a simple predator–prey system varies according to the predator's mean conversion rate.

Entities, state variables, and scales

Agents are of two types: predators and prey. Each agent is characterised by a specific identity number. The agent-level state variables are their two spatial coordinates.

Agents evolve on a two-dimensional, square lattice $\mathcal{L}^2$, whose boundary conditions are periodic, with no apriori limit on the number of agents that can be located in a cell; see section 2.3 for the choice of the lattice parameter values. One time step represents one week and simulations were run for 1000 weeks, i.e. about 19 years.

Process overview and scheduling

At each time step, agents apply a set of rules, whose outcomes depend on random variables and on the local environments, defined as the cell where the agent stands and the eight surrounding cells. One time step corresponds to the implementation of eight modules. First, prey follow the sequence *move*, *reproduce* and *die*. Then predators act in the following order: *move*, *hunt*, *reproduce*, *die* and *migrate*. Within each module, the order between agents is random and updating is asynchronous.

Design concepts

Emergence. The model was formulated so that the emergent behaviour of both population matches the key assumptions of the Rosenzweig-MacArthur model with Allee effect on the prey, cf. section 2.1; namely we expect the prey to exhibit logistic growth and a strong Allee effect, while the predator should collectively exhibit a Holling type II functional response.

Sensing. Each agent can sense the presence of other agents in their local environment.

Interactions. Three types of inter-agent interactions are explicitly modelled. First, prey interact directly through mating: two prey located in the same local environment can give birth to an offspring. Second, prey interact indirectly through density-dependence: mating cannot occur if the number of prey in the local environment exceeds a threshold. Third, predators and prey interact through hunting: predators can hunt the prey located in their local environment.

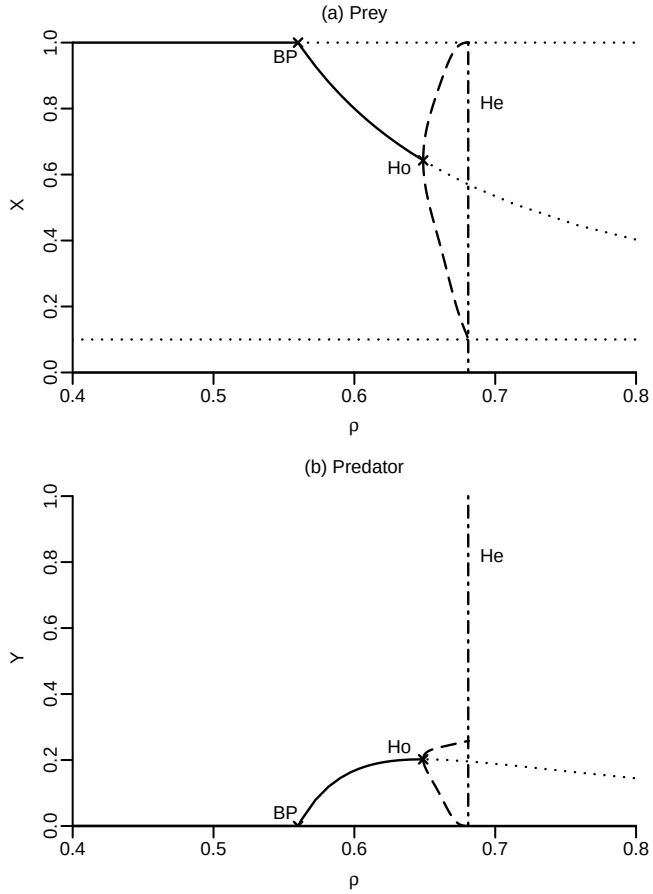

Figure 3: Bifurcation diagram $\mathbf{Z} = \mathbf{Z}(\rho)$ of the ODE model with respect to the parameter ρ, for $A = 0.1$; all the other parameters have the values in Table 1. (a) For the prey population $X = X(\rho)$; and (b) for the predator population $Y = Y(\rho)$. Solid lines represent stable equilibria, dotted lines unstable equilibria. The prey-only fixed point ($X = K, Y = 0$) undergoes a one-sided pitchfork bifurcation, constrained by the positivity of Y, and is denoted in the figure by BP, for branching point; see text for details. This bifurcation from a single to two fixed points is followed by a Hopf bifurcation (Ho), with the dashed lines indicating the extrema of the limit cycles. The vertical dashed line represents the location of the next, global bifurcation, via the birth of a heteroclinic orbit (He); see Fig. 2 (b).

Stochasticity. Many processes involve stochasticity. First, there is spatial stochasticity: The movement of each agent is a two-dimensional random walk on $\mathcal{L}^2$. and each new offspring, prey and predator alike, is assigned to a random location. Next, behaviour is stochastic: Most actions, including breeding, dying, hunting, are probabilistic; specifically, they are realised if a random variable, generally drawn from a uniform distribution between 0 and 1, exceeds a threshold value.

Observation. The main data analysed are the prey and predator populations as a function of time, $X(t)$ and $Y(t)$, respectively.

Initialisation

The model is initialised by setting the initial prey and predator populations, $X(0)$ and $Y(0)$, and by assigning each agent a random location on the lattice $\mathcal{L}^2$. A wide range of initial populations $\mathbf{Z}(0) = (X(0), Y(0))$ was tested during preliminary model exploration. For the simulation experiments reported herein, we chose the initial population pair $(4000, 500)$, which leads to the most interesting dynamics.

Input data

The model does not use input from external models or data files.

Submodels - prey modules

Move — prey move to a randomly selected adjacent cell, whether occupied or not.

Reproduce — When a prey senses at least one other prey in its local environment, and if the local density of prey does not exceed a saturation density S, it has a certain probability b to give birth to another prey. This rule gives rise, at the population level, to two features of the aggregate model: (i) At high density, reproduction is limited by S, which leads to a density-dependent growth rate; and (ii) below a certain density, low mating probabilities lead to extinction. The latter phenomenon corresponds to the Allee effect, cf. Fig. 15 in Appendix A. Offspring are assigned to a random cell; doing so avoids prey immediately mating with their offspring.

Die — Each prey dies with probability v.

Submodels - predator modules

Move — Predators move to a randomly selected adjacent cell, whether occupied or not.

Hunt — When a predator senses prey in its local environment, it has a certain chance s to catch and kill them, but it cannot, in any event, kill more than N prey at a time. This limited handling capacity gives rise, at the population level, to a functional response of type II, cf. Fig. 17 in Appendix A.

Reproduce – After a successful hunt, a predator has a probability κ to breed a number of offspring equal to the number of prey it killed. Like the prey, offspring are randomly located on the lattice. Predators who did not catch any prey cannot breed.

Die — Each predator dies with probability w.

Migrate — If all predators disappear but prey survive, a predator is added to the lattice; this model feature avoids premature disappearance of predators due to purely stochastic phenomena.

2.3. Choice of parameter values

The ABM has eight parameters, one more than the ODE model; these eight parameters are defined, and their values given, in Table 2. The objective choosing a set of parameters for the ABM is to approximate macro-level parameters of the aggregate model with corresponding ratios that emerge from the ABM simulations.

We first focus on the Allee effect. In the ODE model, it is characterised by its intensity, measured by the ratio $A/K = 0.1$. In the ABM, for $L = 100$, $b = 1$, $S = 5$, $v = 0.05$ and $\mathbf{Z}(0) = (4000, 500)$, the average prey population in the absence of predators is denoted by $\hat{K}$ and it equals 6080. This $\hat{K}$ is the emergent carrying capacity, which mirrors the explicitly-defined parameter K in the ODEs.

By carrying out a series of simulations, we also observe that, when the prey population sinks below 520, it is more likely to go extinct than to recover, cf. Fig. 15 in Appendix A. Additional experiments based on feedback control confirm that this value, denoted $\hat{A}$, is the emergent quantity that corresponds to the Allee effect threshold A; see Appendix A for details. We obtain therewith $\hat{A}/\hat{K} = 0.086$, which is close to $A/K = 0.1$ from Table 1.

The functional response, in turn, is characterised in the ODE model by a logistic curve with a half-saturation constant $S = 0.4$. In the ABM, for $s = 0.1$, $M = 3$ and $w = 0.1$, we observe that the average number of prey killed per predator plateaus at 0.3 when prey are abundant, i.e. $X \geq 9000$. When $X = 2750$, the average kill rate is $0.15 = 0.30/2$, which equals the emerging half-saturation constant $\hat{S}$, cf. Fig. 17 in Appendix A. We obtain $\hat{S}/\hat{K} = 0.45$, which is close to $S/K = 0.4$.

Table 2: Summary of the parameters used in the ABM model

Parameter	Definition	Value
L	Number of cells along an edge of the square lattice	100
b	Prey's probability to breed when meeting another prey	1
S	Prey's local saturation density	5
v	Prey's probability to die	0.05
s	Predator's probability to succeed in hunting	0.1
N	Predator's handling saturation	3
κ	Predator's mean conversion rate	$0.21 \leq \kappa \leq 0.7$
w	Predator's probability to die	0.1

2.4. Numerical experiments and analysis methods

We choose the predator's mean conversion rate κ as the bifurcation parameter. For each value of κ between 0.21 and 0.70, in steps of 0.01, we run the model 100 times and monitor the prey population $X(t)$ and predator population $Y(t)$. Each run differs by the realisation of its random choices in agent actions and lasts for $T_\mathrm{f} = 1000$ time steps, i.e. 1000 weeks $\simeq$ 19 years. We obtain a set of $50\times100 = 5000$ time series $X_i^{(\kappa)}(t)$ and $Y_i^{(\kappa)}(t)$, with $\kappa = 0.21, 0.22, \ldots, 0.70$; $i = 1, 2, \ldots, 100$; and $t = 1, 2, \ldots, 1000$. To characterise the dynamics and identify threshold values, we carried out a series of statistical analyses on this output. To deal only with statistically stationary data, we dropped the first 400 points of each time series, so our data set has $5000 \times 600 = 3\,000\,000$ points.

First, for each value of κ, we compute the probability distributions of the corresponding run $X^{(\kappa)}$ and $Y^{(\kappa)}$, and derive the proportion of runs in which prey go extinct (*extinction*), predators go extinct (*prey-only*), or both populations

coexist (*coexistence*). Second, the time series in which the two species coexist were analysed using spectral methods. A few examples of such time series are displayed in Fig. 4.

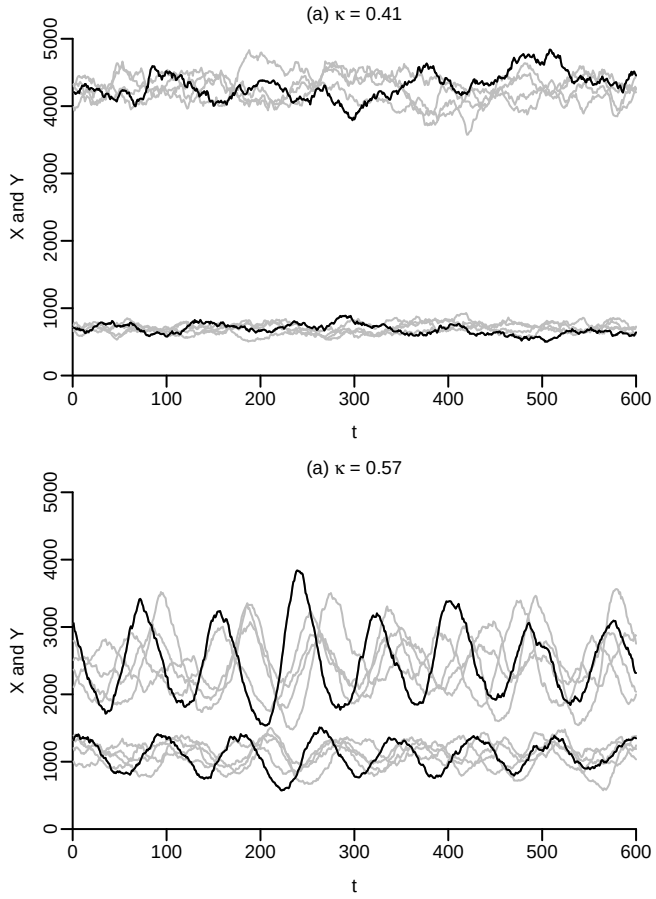

Figure 4: Time series of the prey population $X^{(\kappa)}(t)$ and the predator population $Y^{(\kappa)}(t)$, shown as the upper and lower curves, respectively. Five simulations with $\kappa = 0.41$; and (b) five simulations with $\kappa = 0.57$. In each panel, one of the simulations is shown as the heavy solid curve, the other four as light solid. The fluctuations in panel (a) are more irregular and have smaller amplitudes than those in panel (b). The use of statistical and spectral methods helps locate the transition between these two regime types.

The ABM model was implemented using NetLogo (Wilenski, 1999). The statistical analyses were performed with the R package (R Core Team, 2012).

It is clear from this figure that the behaviour differs widely as a function of parameter value, with $\kappa = 0.41$ in panel (a) and $\kappa = 0.57$ in panel (b). But, because of the stochastic processes that enter agent behaviour, it is difficult to identify the structure of the underlying attractor: Are the irregular fluctuations of the simulated time series mere random noise around a fixed point, or do they exhibit oscillatory behaviour, which would point to a more complex attractor? How can we locate the transition between the two seemingly distinct regimes in Figs. 4a and 4b?

For each value of κ, we analyse the time series in which the two species coexist using singular spectrum analysis (SSA) (Vautard and Ghil, 1989; Vautard et al., 1992; Ghil et al., 2002) and Monte-Carlo SSA (MC-SSA) (Allen

and Smith, 1989; Ghil et al., 2002). These methods have been widely used in climate dynamics and other areas, including population dynamics (Loeuille and Ghil, 1994). They are presented succintly here and more thoroughly in Appendix B.

SSA decomposes a time series into elementary components that can be classified into trends, oscillatory patterns and noise. Each component is associated with an eigenvector and an eigenvalue of the time series's lag-covariance matrix. An oscillation, whether harmonic or anharmonic, is captured by a pair of nearly equal eigenvalues, whose associated eigenvectors have the same dominant frequency and are in phase quadrature. Typically, oscillatory behaviour can be traced back to deterministic processes that contribute to generate the time series under study (Ghil et al., 2002).

MC-SSA tests the SSA results against a null hypothesis that is modelled by a simpler, purely stochastic process which could have generated it, typically white or red noise. Empirical analyses have shown that ecological time series, and in particular population time series, tend to have a 'red-shifted' spectrum (Pimm and Redfearn, 1988). Consequently, we have chosen to test the time series against the more stringent null hypothesis of red noise.

We are interested in detecting statistically significant oscillatory patterns and apply MC-SSA to identify pairs of eigenvalues at the 5% confidence level or better, as explained in Appendix B. Pairs that survive this test will be called significant pairs of eigenvalues (SPEs) and are indicative of oscillations produced by limit cycles, and not by purely stochastic effects.

2.5. Choice of time horizon

Our objective is to identify our predator-prey system's dynamical structure, namely the basins of attractions and bifurcation points. In this perspective, how satisfactory is our choice of $T_\mathrm{f} = 1000$ weeks? To appraise the ecological significance of this time horizon, we evaluate the generation times of the two species, defined as the inverse of the respective death rate. We denote these quantities by T_C for the predator and by T_R for the prey. Since the predator death rate is $w = 0.1\ T_\mathrm{C} = 10$ weeks.

The death rate of the prey is the sum of the natural death rate $v = 0.05$ and a predation rate, while the latter is the product of the average number of prey killed per predator and of the predator abundance; this relationship is represented in Fig. 17 of Appendix A. Since the predator population typically ranges between 0 and 1500, as seen in section 3 below, T_R varies between 8 and 20 weeks. The interval of 1000 weeks used in our study seems, therefore, long enough to capture ecologically significant dynamics, and it suffices in order to avoid the transients due to a choice of initial state alone.

Is this time horizon of 1000 weeks also sufficient in order to account for long-term behaviour? Due to the model's stochastic ingredients, and given long enough simulation intervals, it is quite possible that particular sequences of events that are a priori very unlikely will occur and lead trajectories to change basins of attraction. Since there is no external input of prey, extinction is the only absolutely inescapable regime, into which all trajectories will eventually fall. Focusing on genuinely asymptotic behaviour only would therefore prevent us from identifying the basins of attraction and bifurcation points that, according to the ODE model, do seem to play an important role. The

ecologically significant dynamics might thus lie in what can be considered, from an asymptotic standpoint, as merely very long transients (Hastings, 2004). We carried out additional experiments with $T_\mathrm{f} = 10\,000$ weeks ≈ 200 years and $T_\mathrm{f} = 100\,000$ weeks ≈ 2000 years to assess the robust persistence of each attractor basin identified, along with evaluating associated probabilities.

3. ABM model results

3.1. Dominant regime and fixed points

As in the ODE model, if the initial predator population is large compared to the initial prey population, the prey will go extinct first, followed by the predators. For smaller initial predator populations, several regimes can occur: *extinction*, *prey-only* or *coexistence*, as shown in Fig. 5. As the parameter κ — which measures the reproduction efficiency of the predator — increases, two transitions are detected: the first one between 0.35 and 0.36, where the dominant regime switches from prey-only to coexistence, and the second one between 0.60 and 0.61, where it changes from coexistence to extinction.

During this second transition, we observe a small peak in the number of occurrences of the prey-only regime. In these simulations, the combination of stochastic events with moderate κ values leads to the following scenario: the predators deplete the prey population down to a level close to $\hat{A}$, which is insufficient for predator survival, while the prey population — being freed from predation and with the help of positive stochastic events — is able to persist. For higher κ values, predators deplete the prey population more rapidly, so that it falls well below $\hat{A}$ and thus induces extinction of both populations.

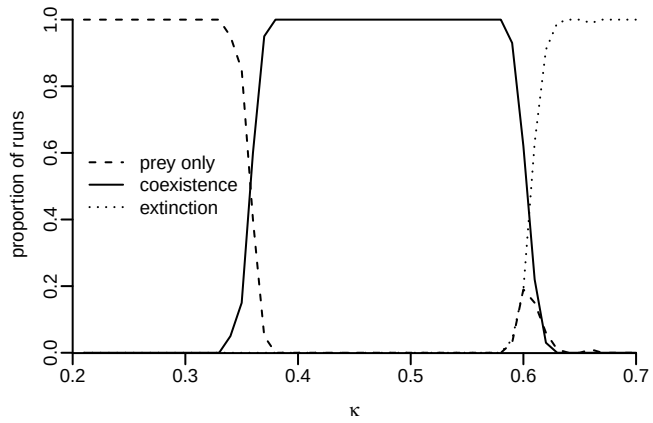

Figure 5: Proportion of ABM runs reaching one of three possible regimes — prey-only (dashed line), coexistence (solid line) or extinction (dotted line) — as the parameter κ varies, $0.21 \leq \kappa \leq 0.70$.

In Fig. 6 we plot, for each κ-value, the distribution of the populations $\{X_i^{(\kappa)}(t)\}$ and $\{Y_i^{(\kappa)}(t)\}$ over the realisations $i = 1, \ldots, 100$, and over the 600-week–long time interval $401 \leq t \leq 1000$. During the first transition, at $\kappa \simeq 0.36$, the

average populations $\overline{\mathbf{Z}}^{(\kappa)} = (\overline{X}^{(\kappa)}, \overline{Y}^{(\kappa)})$ change rather smoothly, whereas the second transition, at $\kappa \simeq 0.61$, is marked by a sudden drop in both population averages. Before the collapse, the range of their values increases rather strikingly.

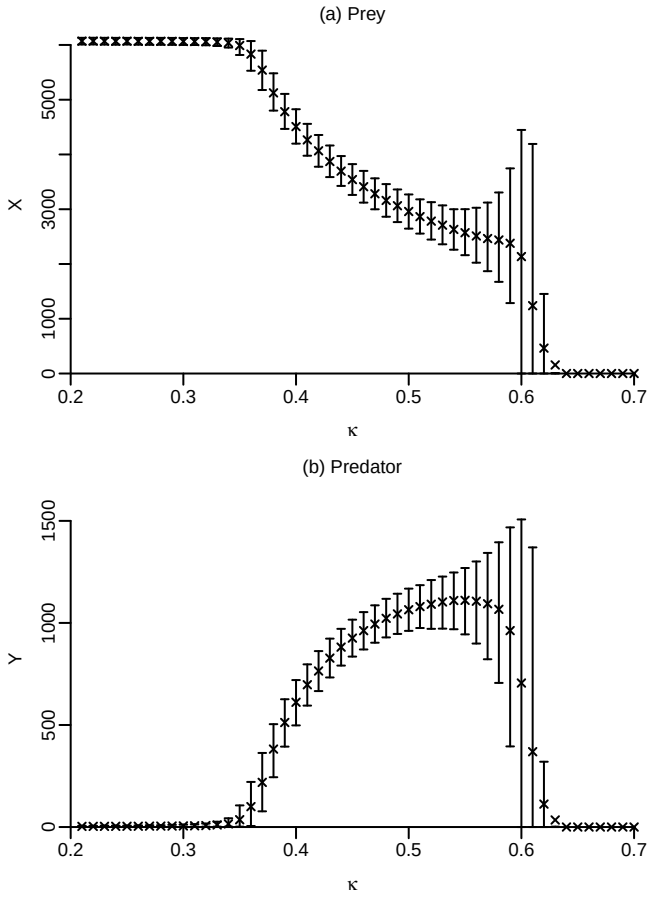

Figure 6: Spread in the set of all population values for ABM model runs, for the realizations $i = 1, 2, \ldots, 100$ and the time interval $401 \leq t \leq 1000$, as a function of κ. (a) For the prey population $\{X_i^{(\kappa)}(t)\}$; and (b) for the predator population $\{Y_i^{(\kappa)}(t)\}$, at each κ-value. The $\times$ symbols indicate the average values $\overline{X}^{(\kappa)}$ and $\overline{Y}^{(\kappa)}$, respectively, of the distributions of $100 \times 600 = 60\,000$ points at each κ, while the bars indicate the interval between the 5^{th} and 95^{th} percentiles of this distribution.

In the prey-only steady state, the prey population fluctuates around $\hat{K} = 6080$ i.e. around a value that is almost 12 times the Allee effect threshold. At this level, only a series of extremely high death rates — combined with very unlikely spatial distributions that severely limit reproduction — could lead the prey towards extinction. The probability of having more than 500 prey dying at once, i.e still a fairly small number that only corresponds to one-eleventh of the road to extinction is less than 10^{-30}. This basin of attraction is so deep that, even on geological time scales, the prey-only regime can be considered as stable.

The coexistence regime requires a more thorough examination. The presence of predators creates new opportunities for adverse stochastic events; still, their probabilities remain extremely low for moderate κ-values. For $\kappa = 0.57$, additional, 2000-year–long simulations still show that less than 2% of the runs lead to extinction. As we approach the

transition at $\kappa \simeq 0.61$, the depth of the basin of attraction decreases and coexistence is less and less likely to persist. Had we initially set the duration of the simulations to 2000 years, rather than 200 years, as in Fig. 6, the transition value of κ would be 0.59 instead of 0.61. This difference is still quite moderate with respect to the size of the basins of attraction, in terms of the parameter κ, as shown in Fig. 5. The robustness of our results upon using longer simulations thus validates our more computationally convenient time horizon of 1000 weeks $\simeq$ 200 years.

By examining, in the two panels of Fig. 7, the probability density function (PDF) of the 100 runs $\times$ 600 points in time of the two simulations at $\kappa = 0.41$ vs. $\kappa = 0.57$, we can distinguish two distinct coexistence regimes. The first regime, in panel (a), is characterised by a well-defined density peak, with lower-density regions falling along a negatively slopped line in the (X, Y) phase plane. This regime corresponds to a fixed point, located at the peak of the PDF, and the negative correlation between prey and predator, away from the peak, reflects the predominance of a top-down regulation (McQueen et al., 1989; Pimm, 1991). The observed negative slope in Fig. 7a is also consistent with the ODE model: near the stable fixed point P_S associated with the coexistence regime, the flow into P_S is tangent to a unique characteristic direction, which has a negative slope; the direction is given by the tangent at P_S to the heteroclinic orbit form the saddle $(K, 0)$; see Fig. 2a.

The second regime, in Fig. 7b, displays no dominant peaks; here, the prey and predator populations are not distributed along a line, but fill a larger area. As we shall see in the next subsection, this regime corresponds to a stochastically perturbed limit cycle.

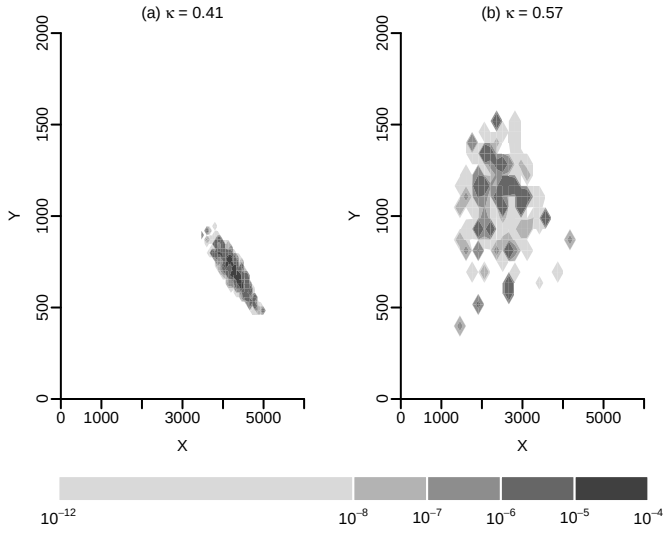

Figure 7: Estimation of the two-dimensional probability density function (PDF), obtained from 100 runs with 600 points each. (a) $\kappa = 0.41$; and (b) $\kappa = 0.57$. The darker the area, the higher the density; see grey bar for shading values.

3.2. *Hopf bifurcation and limit cycle*

To locate the transition between the two coexistence regimes, we apply MC-SSA to the simulated time series with $0.35 \leq \kappa \leq 0.61$, using a set of lag-window lengths M between 80 and 200 weeks, in increments of 20; see Table 3. The transition occurs when MC-SSA identifies at least one SPE in more than 50% of the runs. For all values of M in the table, the numerical results locate the transition in the interval $0.46 \leq \kappa \leq 0.50$. MC-SSA analyses with $M \leq 60$ weeks (not shown) rarely reject the null hypothesis of red noise, because the period of the actual oscillations is larger than M; see Table 4. The transition to a statistically significant SPE is illustrated in Fig. 8 by the statistics of the MC-SSA analyses applied to the predator time series with $M = 120$ weeks.

Results based on prey time series and on predator time series are consistent. In most simulations, only one SPE is detected. The application of MC-SSA thus identifies the emergence of a limit cycle for κ in the transition interval $[0.46, 0.50]$. This transition is equivalent to a Hopf bifurcation. The *oscillatory coexistence* regime lasts from $\kappa = 0.50$ until the transition to the extinction regime, which occurs at $\kappa \simeq 0.60$.

Table 3: Location of the Hopf bifurcation

M	κ-interval (MCSSA on prey)	κ-interval (MCSSA on predator)
80	[0.49, 0.50]	[0.49, 0.50]
100	[0.49, 0.50]	[0.49, 0.50]
120	[0.48, 0.49]	[0.48, 0.49]
140	[0.47, 0.48]	[0.48, 0.49]
160	[0.46, 0.47]	[0.46, 0.47]
180	[0.46, 0.47]	[0.46, 0.47]
200	[0.46, 0.47]	[0.46, 0.47]

Throughout the oscillatory coexistence regime, the average frequency of the limit cycle is $f = 0.012$ cycle/week, i.e. a period of about 83 weeks, cf. Table 4. The choice of M barely impacts the identification of the periods, and the results using prey and predator time series are in satisfactory agreement. We do observe a slight bias towards longer periods for the prey, though.

For instance, for $M = 120$ weeks, in 89% of the runs in which SPEs are detected in both time series, the period associated with the prey is identical to the one associated with the predator. But in 86% of the runs in which the periods are not equal — and especially when κ is close to the transition interval $[0.46, 0.50]$, the prey time series displays a larger period. This difference disappears as κ increases, i.e. as the amplitude of the oscillations increases. While this phenomenon has not specifically been addressed here, a method to investigate it in further work is proposed in section 4.1.

In the steady-state regime, the generation times of the predators and the prey, denoted by T_C and T_R, were 10 weeks

and 8–20 weeks, respectively. In the oscillatory coexistence regime, the period of the oscillations varies between 70 and 94 weeks. This periodicity is consistent with the finding of Murdoch et al. (2002), who established that most consumer–resources cycles exceed $4T_C + 2T_R$.

The transition from steady-state to oscillatory coexistence also becomes apparent when looking at the frequencies of the SPEs. We notice in Fig. 9 that the average frequencies of the few SPEs detected before the transition are several times higher than the average frequencies of the SPEs detected after the transition. This transition from high to low frequencies is also associated with a marked drop in variance. The box-and-whisker diagram (not shown) of the frequencies plotted in Fig. 9 shows that the distributions are markedly asymmetric around the transition, for $0.45 \leq \kappa \leq 0.52$, with the mean lying outside the interquartile range.

The simultaneous jump in period and drop in spread reveals a regime shift between noisy fluctuations around a fixed point — in which rapid and irregular oscillations are detected in a minority of runs, with periodicities between 2 and 20 weeks — and a regular pattern of oscillations with longer periods and larger amplitudes that occur in most runs, with periodicities of 70–94 weeks.

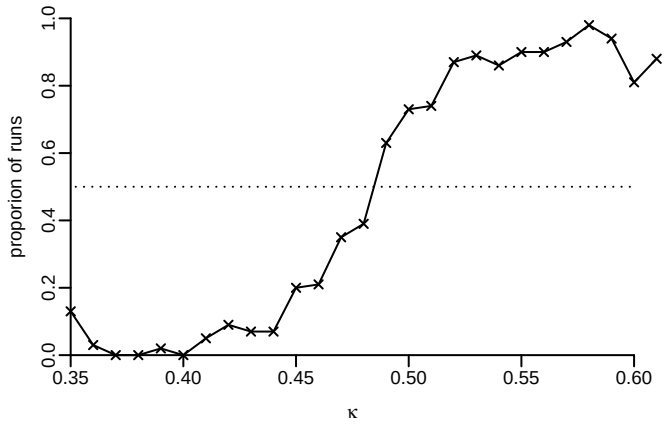

Figure 8: Proportion of runs for which MC-SSA applied to the predator time series yields at least one SPE; $M = 120$ weeks. We locate the transition κ^* at the point at which the curve crosses the 50% threshold, represented as a dotted line; here $0.48 \leq \kappa^* \leq 0.49$.

3.3. Heteroclinic bifurcation

In the ABM, we observe a global bifurcation pattern that does resemble the one found in the aggregate model, cf. section 2.1, and illustrated in particular in Figs 2b and 3: as the limit cycles grow larger, prey have a higher chance to fall below the Allee effect threshold and go extinct, as shown here in Fig. 10. Additional experiments indicate that the actual transition takes place for $0.607 \leq \kappa \leq 0.608$; above this κ-value, extinction occurs in more than half of the runs.

This numerically inferred heteroclinic bifurcation shows two further features: a marked increase of the limit cycle's amplitude (Fig. 6), and period (Fig. 11). These features are present in the ODE model as well — as ρ is increased, the limit cycle that arises from the Hopf bifurcation expands in size and moves closer to the separatrix.

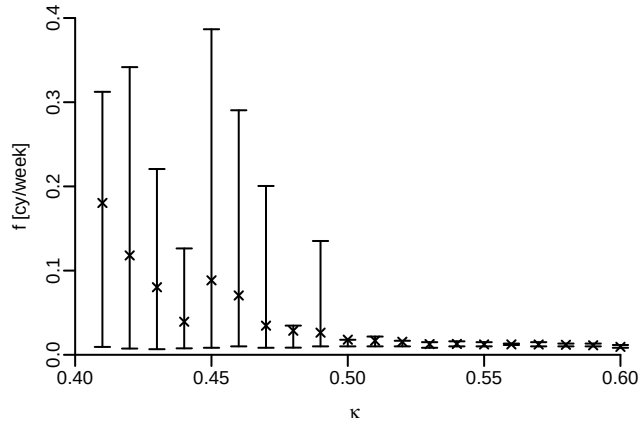

Figure 9: Average frequencies, expressed in cycle per week, associated with the main SPEs detected by MC-SSA on the predator time series for the same $M = 120$ weeks as in Fig. 8. Same symbols for average and spread as in Fig. 6. The average frequencies before the transition, i.e. for $\kappa \simeq 0.48$, are on the average 5 times higher than those after the transition, $0.49 \leq \kappa$, namely 0.063 and 0.012 weeks^{-1}, respectively.

Table 4: Average periods P in weeks and frequencies $f = 1/P$ in cycles/week that are associated with the main SPEs detected via MC-SSA. The entries in the table are computed for κ-values at which SPEs are detected for more than 50% of the runs.

M	P [weeks] ($f = 1/P$) (SSA on prey)	P [weeks] ($f = 1/P$) (SSA on predator)
80	86.2 (0.0116)	80.6 (0.0124)
100	87.7 (0.0114)	84.7 (0.0118)
120	89.3 (0.0112)	80.6 (0.0124)
140	90.1 (0.0111)	76.9 (0.0130)
160	88.5 (0.0113)	80.0 (0.0125)
180	90.1 (0.0111)	78.1 (0.0128)
200	89.3 (0.0112)	78.7 (0.0127)

The associated increase in amplitude is clearly apparent in Fig. 3 for both prey and predator, in panels (a) and (b), respectively.

Another consequence is that the trajectories get closer to the two saddle points, $(A, 0)$ and $(K, 0)$. They approach each one of them along its stable manifold, and move away along the corresponding unstable manifold. In the vicinity of these two saddles, the rate of change becomes exponentially small. Thus, as ρ tends toward the bifurcation point, the system increasingly slows down in the vicinity of the two saddles, and so the period tends towards infinity; see Fig. 12.

In the ABM, the average periodicity associated with the SPEs is nearly constant throughout most of the oscillatory coexistence domain. When κ exceeds 0.58 and approaches the transition point, the periods get longer and longer; see

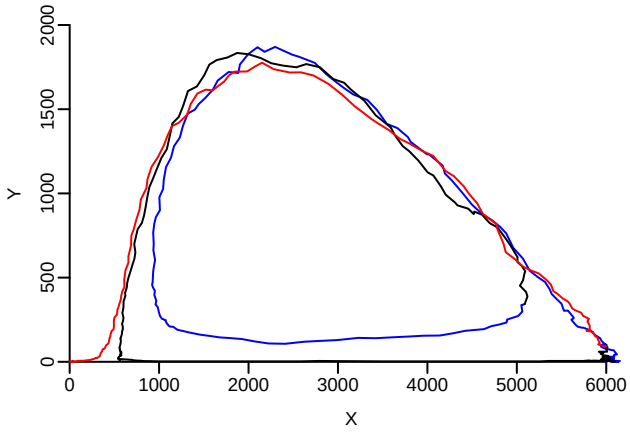

Figure 10: An ABM simulation that illustrates the model's global bifurcation from a stable limit cycle to a single fixed point, via a heteroclinic orbit; in this particular simulation, $\kappa = 0.61$, $X(0) = 6080$ and $Y(0) = 0$. Along this single trajectory, the color changes from blue to black to red, in order to highlight the two transient, nearly closed loops, blue and black, before the red segment that terminates in the origin. The larger, black loop is very similar to the heteroclinic curve of the ODE model in Fig. 2b.

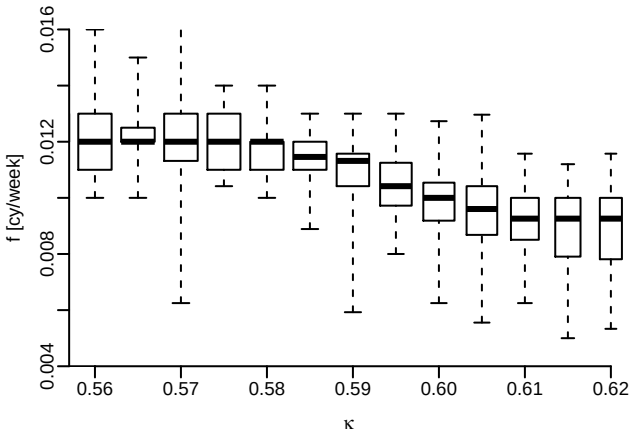

Figure 11: Box-and-whisker diagram of the frequencies, expressed in cycles per week, associated with the main SPEs detected by MC-SSA on the predator time series for $M = 120$ weeks. The bottom and top of the boxes are the first and third quartiles, the heavy horizontal lines inside the boxes are the medians, and the ends of the whiskers are the extrema. The width of a box is proportional to the square root of the number of observations. There is a marked decrease in the frequencies of the SPEs for $\kappa \geq 0.58$. The results for the prey time series exhibit a similar pattern (not shown).

Fig. 11. After the transition, in the few runs where extinction does not occur, the periods keep on increasing, but at a slower pace.

The occurrence of a slowing down in the ABM is consistent with the ODE model. As predators become more efficient, they push the prey towards the Allee effect threshold; see Fig. 13. The fewer prey survive, the slower they find partners and repopulate the lattice. More acute depletions of prey lead to larger depletions of predators, whose recovery is delayed. This delay allows prey to get closer to the carrying capacity, before predators recover. This cycle

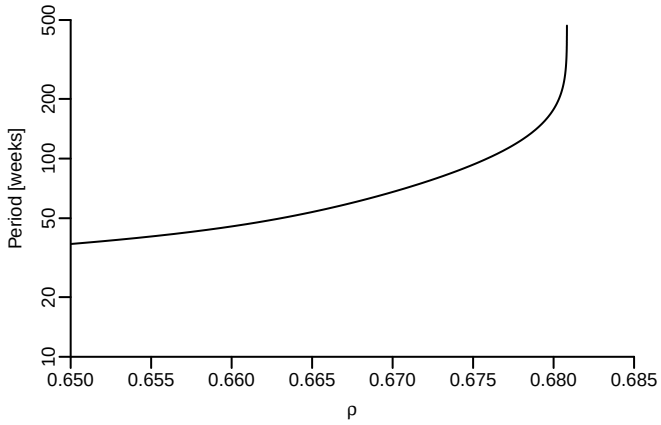

Figure 12: Period of the limit cycle of the ODE model, in log scale, as a function of ρ.

repeats until prey fail to recover and go extinct.

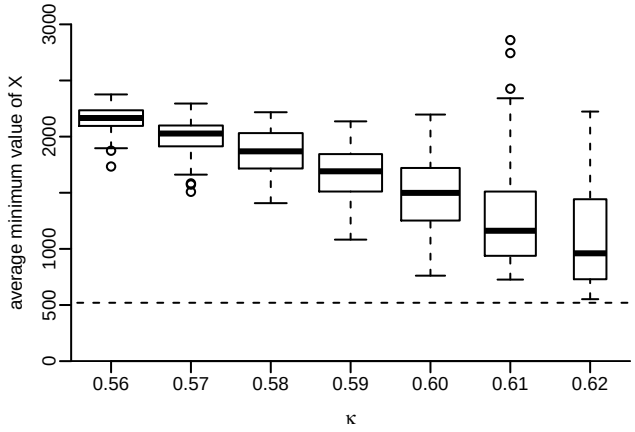

Figure 13: Box-and-whisker diagram of the average minimum prey abundance during oscillations, as a function of κ. Same conventions as in Fig. 11. The horizontal dashed line shows the Allee effect threshold $\hat{A}$.

In contrast to the ODE model, though, the period increases more moderately. Because of the discreteness of the state variables and the resulting demographic stochasticity ~~stochastic processes~~, trajectories do not stay on the limit cycle along which the asyptotic ~~exponential~~ slowing down occurs. They either move back into the hinterland of the coexistence region, where the dynamics is faster, or cross the boundary and fall into extinction. Hence, due to the noise in the ABM, the increase in periodicity remains moderate.

The implications of this slowing-down phenomenon for a potential early warning ahead of the heteroclinic bifurcation will be discussed in section 4.2.

4. Concluding remarks

4.1. Summary and discussion

Even simple ecological systems can exhibit complex dynamics. In this paper, we have shown that an approach based on a hierarchy of models can be highly effective in exploring such a complex system. At one end of the modelling spectrum, ABMs are arguably best adapted for 'realistic' modelling, inasmuch as many observed features of the individuals that are an ecosystem's building blocks can be plugged in directly. We argue that ABMs should, as much as possible, be developed in conjunction with simpler 'toy' models. Doing so facilitates the analysis, allows one to compare results, and finally to draw robust conclusions. This back-and-forth between different models is also well illustrated by Siekmann (2015) in the case of the dynamics of a two-strain infection process.

In this paper, we focused on a simple predator–prey system, using a deterministic ODE model and a stochastic ABM. Running ABM simulations and analysing their output were computationally intensive and time consuming tasks. For instance, the application of MC-SSA required the generation and analysis of 200 surrogate data — 100 for the prey time series, and 100 for the predator time series — for each one of the 100 simulations run per ρ value. Given the 50 ρ values used, this yields $200 \times 100 \times 50 = 10^6$ runs.

Nevertheless, the analysis could be conducted efficiently because it was guided by the existence of a much simpler and, in part, analytically tractable ODE model. The process was quite straightforward in this case, since the ABM model was built a priori to share certain features of the aggregate model. Still, the striking success of the guidance provided by the simpler model suggests that this approach might be of great interest across a richer hierarchy of models.

An interesting addition would be a model of intermediate complexity based on stochastic differential equations (SDEs), which combine some of the stochastic features of ABMs with the simple deterministic ones of ODE models. Bifurcations of nonlinear SDEs have been studied by Kuehn (2011), and their usefulness in the climate modelling hierarchy has been demonstrated by Ghil et al. (2008) and Chekroun and Ghil (2011), among others. In particular, SDEs could be used to explore the possible stochastic origin of the bias towards larger periodicities of the prey time series observed in Tab. 4. An explanation might be that stochastic perturbations occasionally block the oscillations of the prey population, leading to larger average periods. To investigate this hypothesis, one could perturb the deterministic aggregate model by adding multiplicative noise — first to one ODE at a time, then to both.

The guidance provided by the ODE model helped us decide on which parameter to control and which bifurcations to expect. But to actually perform the analysis, we needed to carefully design simulation experiments and develop or adapt appropriate statistical methodology. Simple tests were used to detect transitions between the main regimes. For more challenging tasks, such as the detection of the Hopf bifurcation, we tapped into well-established methods of time series analysis. The advanced spectral methods of SSA and its derivatives were used to distinguish large-amplitude, regular and stable oscillations from small-amplitude, irregular fluctuations. A statistical test based on a Monte Carlo algorithm was used to identify oscillatory patterns that significantly differ, at the 5% level, from a red noise process.

Whether applied to the predator or to the prey time series, the analysis indicates a similar location of the Hopf bifurcation, which in addition was robust to changes of the window-width. The transition region from steady states to oscillatory behaviour was also marked by a sharp decrease in the mean and variance of the oscillations' frequencies; this decrease provides further evidence for a transition from a regime of small, rapid and erratic fluctuations to a regime of ample, regular and stable oscillations. MC-SSA thus appears to be well-suited for the detection and analysis of oscillatory dynamics in ABM-simulated time series.

Further methods of time series analysis could be integrated into the toolbox of ABM users. For instance, Kolmogorov entropy or Lyapunov exponents could provide further insights into whether a deterministically chaotic process has participated in generating a given time series (Kantz, 1994; Schouten et al., 1994). The application of such observables to experimental time series is often hampered by the limited length and accuracy of such series; this impediment does not exist for ABM-generated output.

Time series analysis alone does, however, not take advantage of the modeller's ability to freely design simulation experiments. The application of control-based methods — such as the one used to locate the Allee effect threshold, see Appendix A — seems to be a promising approach for the dynamical analysis of ABMs. Besides, Kevrekidis and colleagues have developed an 'equation-free' approach, in which macroscopic variables and their derivatives are obtained from microscopically defined models — such as ABMs — through the systematic implementation of a set of appropriately initialised simulations (Kevrekidis et al., 2004). This *coarse-graining* process enables one to use numerical bifurcation methods and it was applied to ABMs describing an epidemiological network (Reppas et al., 2010) and a financial market (Siettos et al., 2012).

Our approach to bifurcation in ABMs conceptually differs from the classic mathematical framework for bifurcation analysis in ODEs. In the latter, bifurcations are precisely defined using the same type of mathematical objects as those used to build the model. For instance, Hopf bifurcations can be precisely detected through the application of the Poincaré-Andronov-Hopf theorem. When needed, numerical methods are employed to compute the local structure of the Jacobian matrix and identify a bifurcation. Bifurcations are, in other words, endogenous to the model.

In this paper we used MC-SSA and defined the Hopf bifurcation as the point at which, in a majority of simulations, we observed the emergence of oscillations that are different from a red noise, at a preset significance level. In this approach, the analytical method used is as important as the ABM formulation for the analysis of the bifurcations.

4.2. Early warnings of a global bifurcation

Studying a hierarchy of models is also instructive in testing results on critical transitions and their ex-ante detection through 'early-warning signals'. The heteroclinic bifurcation present in both of our models belongs to the class of global bifurcations, which are structurally unstable and hence harder to detect numerically (Hale and Koçak, 1991). Moreover, Scheffer et al. (2009) and Boettiger et al. (2013) noted, in fact, that the early-warning signals of such bifurcations have been studied relatively little: most early-warning signals proposed in the literature — namely slowing down of trajectories, as well as increased variance, autocorrelation and skewness — derive from the properties of the

saddle-node bifurcation, which belongs to the class of local bifurcations (Hale and Koçak, 1991).

In section 3.3 we have seen that, in both models, some key features of the limit cycles change as the system approaches the heteroclinc bifurcation. The limit cycles get closer to the boundary of the basin of attraction, their amplitudes increase, and the oscillations slow down as a result of approaching the infinite period of the exact heteroclinic orbit.

This type of period increase differs from the phenomenon known as critical slowing down (CSR) (Wissel, 1984; Nes and Scheffer, 2007). The latter refers to the increase of return time after perturbations near a threshold, due to the real part of the dominant eigenvalue of a fixed point approaching zero. CSR has been theoretically demonstrated, and empirically tested, for a range of local bifurcations, especially for saddle-node bifurcations (Boettiger et al., 2013), and it is interpreted as a loss of resilience in the vicinity of a tipping point (Nes and Scheffer, 2007; Dai et al., 2012).

In the ODE model, after the Hopf bifurcation, the unstable fixed point of region (4) of Fig. 1 becomes more repellent as ρ increases, and the geometry of the flow near it changes. As a consequence, trajectories become gradually more affected by the specific dynamics that occurs in the vicinity of the two saddle points, $(A, 0)$ and $(K, 0)$. The slowing down does not originate from the real part of any eigenvalue vanishing; instead, it is due to a geometrical change of the basin of attraction. Another difference with respect to CSR is that this phenomenon is not observed through exogenous perturbations, but affects the endogenous dynamics of the system, i.e. the limit cycle. Even so, a broad-brush interpretation that is similar to CSR could be proposed, namely, as the parameter ρ — which is the conversion rate of the predator — increases, each population, which is periodically perturbed by the other one, recovers more and more slowly, i.e. it is less resilient.

The system as a whole is also less resilient, as it lies closer to the boundary of the basin of attraction, i.e. it is more 'precarious', in the sense of Walker et al. (2004). This aspect is more adequately captured by the amplitude of the limit cycles, to be compared with some known boundaries of the basin, such as the Allee effect threshold.

The slowing down near the two saddle points is also expected to induce an asymmetry in the distribution of the population abundance. This asymmetry can be captured by computing the skewness of the probability distribution in the time series. Guttal and Jayaprakash (2008) have proposed skewness γ as a potential early-warning signal for local bifurcation: γ is simply a distribution's third standardised moment, and it measures its degree of asymmetry. Given a random variable Z, with mean μ and standard deviation σ, skewness γ is defined as

$$\gamma = E\left[\left(\frac{Z-\mu}{\sigma}\right)\right]. \tag{2}$$

Results presented in Fig. 14 show that, in the ODE model, the asymmetry of both trajectories markedly increases as ρ approaches the bifurcation value 0.6801. The system slows down in regions with few predators, and accelerates when predators are abundant, so that the oscillations of the predator population is unbalanced towards low values. We can show analytically that, due to the strong Allee effect, prey recovery near $(A, 0)$ is much quicker than predator recovery near $(K, 0)$. As a consequence, the slowing down near $(K, 0)$ is more marked than the slowing down near $(A, 0)$, and the prey distribution tends to be unbalanced towards high values. While Guttal and Jayaprakash (2008)

applied skewness to study perturbed trajectories around a fixed point in the vicinity of a local bifurcation, we see in Fig. 14a that this measure can also be used for oscillatory regimes approaching a global bifurcation, but for different dynamical reasons.

Skewness results for the ABM differ widely from the ODE ones; see Fig. 14b. Before the transition, which occurs for $\kappa \simeq 0.60$, the skewness of predator time series moderately increases in average, but we do not observe a decrease for the prey time series. Moreover, the signs of the skewness seem surprising with regards to the ODE results. This points out at one major difference between the two models. In the ABM, the mating requirements for prey, which is not modelled in the ODE, significantly slows down the systems in the $(\hat{A}, 0)$ region. In the ODE, the situation is opposite: because of the strong Allee effect, the growth rate of the prey in the $(A, 0)$ region is higher than in the other regions. The two models therefore exhibits opposite results.

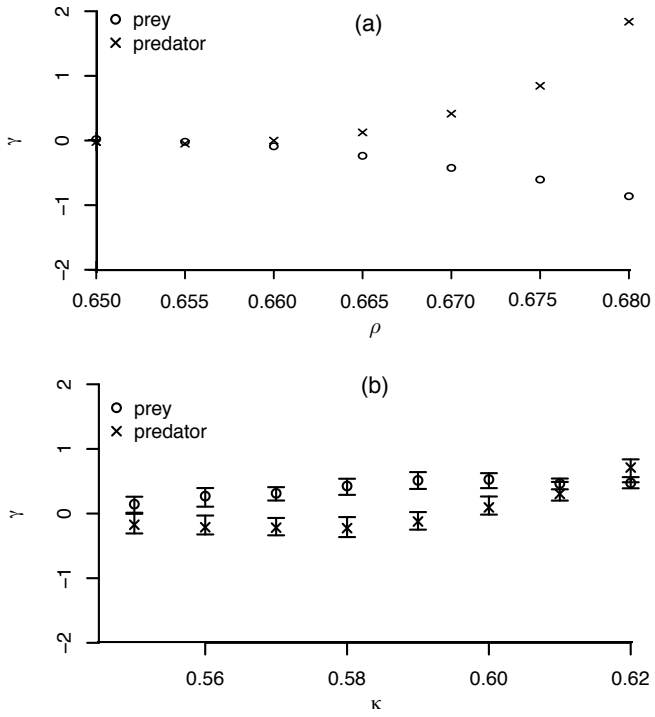

Figure 14: Skewness γ of the predator and prey time series (a) in the ODE model as a function of ρ; and (b) in the ABM model as a function of κ. In panel (b), the vertical bar represents the interquartile range.

The preceding discussion stresses an interesting slowing down phenomenon, which is different from CSR but, like it, also has considerable potential as an early warning signal. Skewness, however, seems to be more ambiguous as a signal, since its behaviour differs between the aggregate model and the ABM. This discrepancy allowed us to identify rather subtle differences in in the formulation of the two models. By using a hierarchy of models, we are, therewith, able to precisely understand the role of each mechanism in the overall dynamics.

4.3. Exogenous and endogenous changes of parameter values

In the ABM, the analyses were carried out for fixed κ-values that are kept constant over the duration of a run. This type of analysis can remain valid for rates of change of κ that are slow compared to the characteristic times of the system's endogenous dynamics, i.e. in the 'adiabatic limit'. We sketch now two possible applications in which κ varies with time.

The simplest application is to add an exogenous rate of change $c = \text{const.}$ for $\kappa(t)$. This scenario could help one study the effect of external forcing that varies smoothly on an ecosystem or a community of species. Rising temperatures have a direct effect on the metabolism, physiology and phenology of organisms; see for instance Bale et al. (2002) for insect herbivores. Exogenously increasing κ can model, for instance, a situation in which rising temperatures tend to increase the predators' reproductive efficiency. We performed additional simulations with $\kappa(0) = 0.55$ and various c-values.

When $c \leq 10^{-5}\kappa$-unit/week, the results obtained in sections 3 and 4.2 still apply. Both populations go extinct for $\kappa \simeq 0.60$, and this extinction is preceded by a marked increase in the amplitudes and periods of the oscillations. For higher rates of change, extinction occurs more rapidly and fewer oscillations are observed, but it tends to occur for a higher κ-value. For instance, with $10^{-5} < c \leq 10^{-4}\kappa$-unit/week, the prey population crosses the Allee effect threshold after 17 years, on average, and about ten oscillations are observed. While this number of oscillations suffices in order to observe their increase in amplitude, the increase in period cannot be robustly established.

Another application is to introduce a process which internally modifies κ. We use an evolutionary framework, and set κ as the evolving trait. Instead of being exogenous and common to all predators, we turn this parameter into an endogenous agent-level variable, that predators hand down to their offspring. The transmission process occurs with an additive white noise, characterised by its standard deviation σ. The starting κ-value is set to 0.55 for all predators, and the initial prey and predator abundances are set to (2500, 1400), respectively, in the vicinity of the limit cycle.

In this formulation, the average κ-value of the predator population increases. Predators with higher reproduction efficiency always tend to invade, driving the system to extinction, a situation referred to as evolutionary suicide (Gyllenberg et al., 2002; Ferrière, 2009). With $\sigma = 10^{-3}$, and using 100 repetitions, extinction is reached on average after 85 years, and the final average κ-value is 0.61, as in Fig. 6. Here the average κ varies linearly in time, although some runs exhibit phases of acceleration and deceleration. The amplitude and period of the oscillations increase, as expected. Note that in some runs, prey succeed to survive and repopulate the lattice, which corresponds to the small peak identified in Fig. 5.

4.4. Conclusions

We have built an ABM that reproduces the key mechanisms of the Rosenzweig-McArthur model with strong Allee effect on the prey; the mechanisms of interest are the density-dependent growth rate of the prey and the Allee effect on it, as well as the Holling type II function response of the predator. The bifurcation analysis of the classic ODE model shows that the system can exhibit bistability between extinction and either a prey-alone or a coexistence regime. A

Hopf bifurcation divides the coexistence regime into steady-state and oscillatory coexistence. Bistability collapses into a single fixed point through a global bifurcation: the limit cycle becomes an heteroclinic orbit and merges with the separatrix between the two attractors.

The ABM displays the same qualitative behaviour as the aggregate model. Early-warning signals of the critical transition associated with the heteroclinic orbit include the increase in the amplitude and periodicities of the oscillations of both populations.

The study of the ABM was guided by knowledge of the ODE model's behaviour. Going back and forth between the two models allowed us to identify and describe the role of each mechanism, as well as testing the robustness of assumptions about early-warning signals. The solid understanding of the system's dynamical structure can then be used to evaluate the response of the system to parameter changes, whether these changes are exogenous or endogenous.

The ABM's bifurcations were detected through the use of of singular spectrum analysis (SSA) and its derivatives. We argue that ABM practionners facing noisy and seemingly oscillatory responses may benefit from methods of time series analysis. We showed that MC-SSA can reliably detect the transition corresponding to Hopf bifurcation. Studying their Lyapunov exponents and the Kolmogorov entropy could also be of interest in assessing the chaotic behaviour of an ABM-generated process.

We further argue that jointly developing models of different level of complexity, from simple 'toy' models to detailed 'realistic' models, is an appropriate approach to study complex ecological systems. Such a hierarchical approach can effectively guide single-model exploration, help cross-check results, and derive more robust conclusions.

Acknowledgements. It is a pleasure to thank Régis Ferrière and the Ecologie-Evolution (EcoEvo) team from the Ecole Normale Supérieure for discussions and suggestions. Particular thanks are due to Andreas Groth and the Theoretical Climate Dynamics (TCD) group of the University of California at Los Angeles for their help on implementing and applying SSA. This work was supported by a Monge Fellowship of the Ecole Polytechnique (C.C.), by the Agence Nationale de la Recherche through grant PHYTBACK (ANR-10-BLAN-7109) (D.C.), and the European Union project ENSEMBLES (M.G.)

Appendix A. Choice of parameter values

In this appendix, we illustrate the connection between certain local rules used in our ABM modelling of section 2.2 and the aggregate properties of our ODE model in section 2.1. Thus Fig. 15 shows that, below a population of $X = 520$ the prey is more likely to become extinct than not. To confirm that this value is associated with the Allee effect threshold $\hat{A}$, we conducted an additional set of experiments based on feedback control, as suggested by an anonymous reviewer.

In the ODE model, $(X = A, Y = 0)$ is an unstable equilibrium that lies on the $X-$axis. To locate this point in the ABM, we run at each time step — after implementing all the other procedures in the ODD protocol described in section 2.2 — a feedback procedure that artificially maintains the prey population at a given value, denoted by X_S.

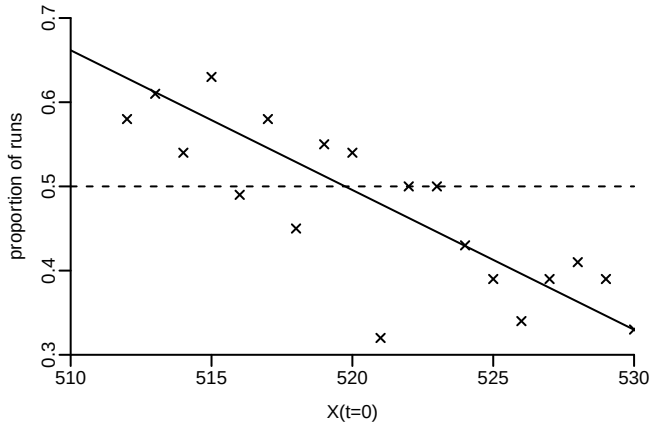

Figure 15: Proportion of predator-free runs, $Y(0) = 0$, in which prey go extinct as a function of the initial number of prey $X(0) \neq 0$. The $\times$ symbols are the outcomes of numerical simulations, the dashed horizontal line indicates the 50% threshold, and the solid line is the result of linear regression. The two straight lines are used to determine the emerging Allee effect threshold $\hat{A}$.

This procedure performs the following tasks: if $X > X_S$, $X - X_S$ prey are randomly removed; conversely, if $X < X_S$, $X - X_S$ prey are randomly added. The asymptotic mean value of $X - X_S$, denoted by $U(X_S)$, measures the sign and the intensity of the feedback that maintain the prey population at X_S. Figure 16 shows that $U(X_S)$ equals zero when $X_S = 520$ and that it changes sign at this point: when $X_S < 520$, on average, individuals have to be added to maintain the population, while for $X_S < 520$, on average, individuals have to be removed. This result precisely locates the value of $\hat{A} = 520$, which leads in turn to the ABM's emergent $\hat{A}/\hat{K} = 0.086$ being a good approximation to the aggregate model's pre-defined $A/K = 0.1$; see section 2.2 for details.

The effectiveness of this method at identifying the saddle node suggests further explorations of the potential applications of control-based approaches for the study of ABMs and their dynamics. It could in particular be employed to perform numerical continuation of unstable equilibria or to track periodic solutions, as demonstrated by Barton (2013) for physical experiments..

The intersection of the horizontal dash-dotted line in Fig. 17 with the dotted vertical line at $X = 2750$ gives the ABM's emerging half-saturation constant $\hat{S}$ and, therewith, an emerging $\hat{S}/\hat{K} = 0.45$, which is close to the aggregate model's $S/K = 0.4$; see section 2.2 for details.

Appendix B. Singular spectrum analysis (SSA)

The SSA methodology involves three basic steps: (1) embedding a time series $\{X(t) : t = 1, 2, \ldots, N\}$ of length N in a vector space of dimension M — for the choice of M, see Vautard et al. (1992) and Ghil et al. (2002); (2) computing the $M \times M$ lag-covariance matrix C_{D} of the data — see the two different approaches of Broomhead and

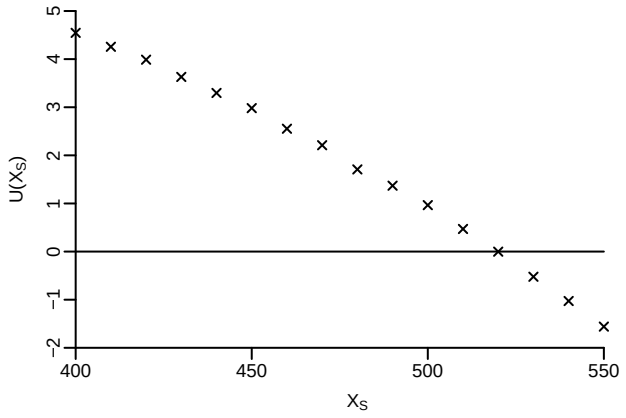

Figure 16: Average feedback intensity that needs to be applied to the prey after each iteration to maintain the population at X_S. This quantity is the average value of $X(t) - X_S(t)$ for $10\,001 \le t \le 20\,000$. Each points correspond to the average value computed for 10 runs; see text for details.

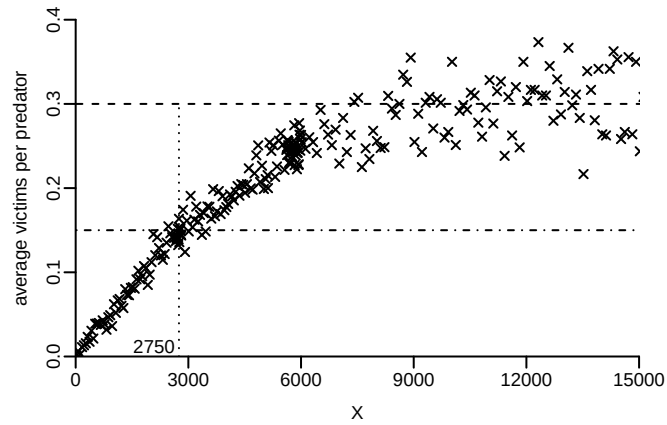

Figure 17: Average number of prey killed per predator, as a function of prey population X. The horizontal dashed line shows the saturation value of 0.3 that is attained at roughly $X = 9000$, while the dash-dotted horizontal line corresponds to the half-saturation point at 0.15; the latter is attained at the value $X = 2750$, which is indicated by the dotted vertical line.

King (1986) and Vautard and Ghil (1989); and (3) diagonalizing C_D:

$$\Lambda_\mathrm{D} = E_\mathrm{D}^T C_\mathrm{D} E_\mathrm{D}; \tag{B.1}$$

here $\Lambda_\mathrm{D} = \mathrm{diag}(\lambda_1, \lambda_2, \ldots \lambda_M)$, with $\lambda_1, \lambda_2, \ldots \lambda_M > 0$ the real, positive eigenvalues of the symmetric matrix C_D, and E_D is the $M \times M$ matrix having the corresponding eigenvectors $\mathbf{E}_\kappa$, $\kappa = 1, \ldots M$, as its columns.

For each $\mathbf{E}_\kappa$ we construct the time series of length $N - M + 1$, called the κ-th principal component (PC); this PC represents the projection of the original time series on the eigenvector $\mathbf{E}_\kappa$, also called empirical orthogonal function (EOF). Each eigenvalue λ_κ gives the variance of the corresponding PC; its square root is called a singular value.

The Monte Carlo version of SSA (MC-SSA) is used to reliably identify oscillations in a time series (Allen and Smith, 1989; Ghil et al., 2002). In MC-SSA, one assumes a simple, random model for the analysed time series, referred to as the null hypothesis. We choose an autoregressive process $Z(t)$ of order one, also called a red noise, as the null hypothesis. The process $Z(t)$ solves

$$Z(t) = a_1[Z(t-1) - Z_0] + \sigma\xi(t) + Z_0, \tag{B.2}$$

where a_1, Z_0 and σ are parameters and ξ is a normally distributed white noise of mean 0 and variance 1. For each time series $X(t)$, the three parameters of the corresponding $Z(t; a_1, Z_0, \sigma)$ are computed by maximum-likehood fitting.

Next, a Monte Carlo ensemble of surrogate time series is generated from the null hypothesis and SSA is applied to the data and to the surrogates, to test whether it is possible to distinguish the original time series from the surrogates. Specifically, the $M \times M$ lag-covariance matrix of the Monte Carlo ensemble is projected onto the EOFs of the analysed time series, and one computes the statistics of the diagonal elements of the projected matrices. If the eigenvalue of a specific EOF of the analysed time series is larger than 95% of the corresponding diagonal elements computed from the surrogates, then the null hypothesis is rejected with a 95% confidence level.

Ghil et al. (2002) provide an overview and a comprehensive set of references; see also their free software at http://www.atmos.ucla.edu/tcd/ssa/.

References

Allen, M., Smith, L., 1989. Monte carlo ssa: Detecting irregular oscillations in the presence of coloured noise. J. Climate 9, 3373–3404.

Bale, J. S., Masters, G. J., Hodkinson, I. D., Awmack, C., Bezemer, T. M., Brown, V. K., Butterfield, J., Buse, A., Coulson, J. C., Farrar, J., Good, J. E. G., Harrington, R., Hartley, S., Jones, T. H., Lindroth, R. L., Press, M. C., Symrnioudis, I., Watt, A. D., Whittaker, J. B., 2002. Herbivory in global climate change research: direct effects of rising temperature on insect herbivores. Glob. Change Biol. 8 (1), 1–16.

Barton, D. A. W. Sieber, J., 2013. Systematic experimental exploration of bifurcations with noninvasive control. Phys. Rev. E 87 (5), 052916.

Boettiger, C., Ross, N., Hastings, A., 2013. Early warning signals: The charted and uncharted territories. Theor. Ecol. 6 (3), 255–264.

Bonabeau, E., 2002. Agent-based modeling: Methods and techniques for simulating human systems. Proceedings of the National Academy of Sciences of the United States of America 99, 7280–7287.

Boukal, D. S., Sabelis, M. W., Berec, L., 2007. How predator functional responses and Allee effects in prey affect the paradox of enrichment and population collapses. Theor. Popul. Biol. 72 (1), 136–147.

Broomhead, D., King, G., 1986. Extracting qualitative dynamics from experimental data. Physica D 20, 217–236.

Chekroun, M. D., E. S., Ghil, M., 2011. Stochastic climate dynamics: Random attractors and time-dependent invariant measures. Physica D 240 (21), 1685–1700.

Crowl, T. A., Crist, T. O., Parmenter, R. R., Belovsky, G., Lugo, A. E., 2008. The spread of invasive species and infectious disease as drivers of ecosystem change. Front. Ecol. Environ. 6 (5), 238–246.

Dai, L., Vorselen, D., Korolev, K. S., Gore, J., 2012. Generic indicators for loss of resilience before a tipping point leading to population collapse. Science 336 (6085), 1175–1177.

De Roos, A. M., Persson, L., 2005. Unstructured population models: do general assumptions yield general theory? In: Cuddington, K., Beisner, B. (Eds.), Ecological Paradigms Lost: Routes of Theory Change. Theoretical Ecology Series. Elsevier Academic Press, Burlington, MA, USA, pp. 31–62.

DeAngelis, D. L., Mooij, W. M., 2005. Individual-based modeling of ecological and evolutionary processes. Annu. Rev. Ecol. Evol. S. 36 (1), 147–168.

Dhooge, A., Govaerts, W., Kuznetsov, Y. A., 2003. Matcont: A Matlab package for numerical bifurcation analysis of ODEs. ACM Trans. Math. Software 29, 141–164.

Dieckmann, U., Law, R., Metz, J. A. J., 2000. The Geometry of Ecological Interactions: Simplifying Spatial Complexity. Cambridge University Press.

Dijkstra, H. A., Ghil, M., 2005. Low-frequency variability of the large-scale ocean circulation: A dynamical systems approach. Rev. Geophys. 43, RG3002.

Donalson, D. D., Nisbet, R. M., 1999. Population dynamics and spatial scale: effects of system size on population persistence. Ecology 80 (8), 2492–2507.

Durrett, R., Levin, S., 1994. The importance of being discrete (and spatial). Theor. Popul. Biol. 46 (3), 363–394.

Ferrière, R., 2009. Evolutionary Conservation Biology, 1st Edition. Cambridge University Press, Cambridge, UK.

Fussmann, G. F., Ellner, S. P., Shertzer, K. W., Jr, N. G. H., 2000. Crossing the Hopf bifurcation in a live predator-prey system. Science 290 (5495), 1358–1360.

Ghil, M., 2001. Hilbert problems for the geosciences in the 21st century. Nonlinear Proc. Geoph. 8, 211–222.

Ghil, M., Allen, M. R., Dettinger, M. D., Ide, K., Kondrashov, D., Mann, M. E., Robertson, A. W., Saunders, A., Tian, Y., Varadi, F., Yiou, P., 2002. Advanced spectral methods for climatic time series. Rev. Geophys. 40 (1), 3–1–3–41.

Ghil, M., Chekroun, M. D., Simonnet, E., 2008. Climate dynamics and fluid mechanics: Natural variability and related uncertainties. Physica D 237, 2111–2126.

González-Olivares, E., González-Yañez, B., Mena-Lorca, J., Ramos-Jiliberto, R., 2006. Modelling the allee effect: are the different mathematical forms proposed equivalents? In: Mondaini, R. (Ed.), Proceedings of the 2006 International Symposium on Mathematical and Computational Biology BIOMAT 2006.

Gras, R., Devaurs, D., Wozniak, A., Aspinall, A., 2009. An individual-based evolving predator-prey ecosystem simulation using a fuzzy cognitive map as the behavior model. Artif. Life 15 (4), 423–463.

Grimm, V., Berger, U., Bastiansen, F., Eliassen, S., Ginot, V., Giske, J., Goss-Custard, J., Grand, T., Heinz, S. K., Huse, G., Huth, A., Jepsen, J. U., Jørgensen, C., Mooij, W. M., Müller, B., Pe'er, G., Piou, C., Railsback, S. F., Robbins, A. M., Robbins, M. M., Rossmanith, E., Rüger, N., Strand, E., Souissi, S., Stillman, R. A., Vabø, R., Visser, U., DeAngelis, D. L., 2006. A standard protocol for describing individual-based and agent-based models. Ecol. Model. 198 (1-2), 115–126.

Grimm, V., Berger, U., DeAngelis, D. L., Polhill, J. G., Giske, J., Railsback, S. F., 2010. The ODD protocol: A review and first update. Ecol. Model. 221 (23), 2760–2768.

Grimm, V., Railsback, S. F., 2005. Individual-based Modeling and Ecology. Princeton University Press, Princeton.

Grimm, V., Wyszomirski, T., Aikman, D., Uchmański, J., 1999. Individual-based modelling and ecological theory: synthesis of a workshop. Ecol. Model. 115 (2–3), 275–282.

Guttal, V., Jayaprakash, C., 2008. Changing skewness: an early warning signal of regime shifts in ecosystems. Ecol. Lett. 11 (5), 450–460.

Gyllenberg, M., Parvinen, K., Dieckmann, U., 2002. Evolutionary suicide and evolution of dispersal in structured metapopulations. J. Math. Biol. 45 (2), 79–105.

Hale, J. K., Koçak, H., 1991. Dynamics and Bifurcations. No. 3 in Texts in Applied Mathematics. Springer-Verlag, New York.

Hastings, A., 1990. Spatial heterogeneity and ecological models. Ecology 71 (2), 426–428.

Hastings, A., Jan. 2004. Transients: the key to long-term ecological understanding? Trends Ecol. Evol. 19 (1), 39–45.

Kantz, H., 1994. A robust method to estimate the maximal Lyapunov exponent of a time series. Phys. Lett. A 185 (1), 77–87.

Kevrekidis, I. G., Gear, C. W., Hummer, G., 2004. Equation-free: The computer-aided analysis of complex multiscale systems. AIChE J. 50 (7), 1346–1355.

Kuehn, C., 2011. A mathematical framework for critical transitions: Bifurcations, fast–slow systems and stochastic dynamics. Physica D 240 (12), 1020–1035.

Lavergne, S., Mouquet, N., Thuiller, W., Ronce, O., 2010. Biodiversity and Climate Change: Integrating Evolutionary and Ecological Responses of Species and Communities. Annu. Rev. Ecol. Evol. S. 41 (1), 321–350.

Law, R., Dieckmann, U., 2000. Moment approximations of individual-based models. In: Dieckmann, U., Law, R., Metz, J. A. (Eds.), The Geometry of Ecological Interactions: Simplifying Spatial Complexity. Cambridge University Press, Cambridge, p. 252–270.

Lindegren, M., Möllmann, C., Nielsen, A., Brander, K., MacKenzie, B. R., Stenseth, N. C., 2010. Ecological forecasting under climate change: the case of Baltic cod. P. Roy. Soc. Lond. B Bio.

Loeuille, N., Ghil, M., 1994. Intrinsic and climatic factors in North-American animal population dynamics. BMC Ecology 4 (6), 12 pp.

Mccauley, E., Wilson, W. G., De Roos, A. M., 1993. Dynamics of age-structured ad spatially structured predator-prey interactions: individual-based models and population-level formulations. Am. Nat. 142 (3), 412–442.

McQueen, D. J., Johannes, M. R. S., Post, J. R., Stewart, D. J., Lean, D. R. S., 1989. Bottom-up and top-down impacts on freshwater pelagic community structure. Ecol. Monogr. 59 (3).

Murdoch, W. W., Kendall, B. E., Nisbet, R. M., Briggs, C. J., McCauley, E., Bolser, R., 2002. Single-species models for many-species food webs. Nature 417 (6888), 541–543.

Nes, E. H. v., Scheffer, M., 2007. Slow recovery from perturbations as a generic indicator of a nearby catastrophic shift. Am. Nat. 169 (6), 738–747.

Pimm, S. L., 1991. The balance of nature? University of Chicago Press, Chicago, Illinois, USA.

Pimm, S. L., Redfearn, A., 1988. The variability of population densities. Nature 334 (6183), 613–614.

R Core Team, 2012. R: A Language and Environment for Statistical Computing. R Foundation for Statistical Computing, Vienna, Austria, `http://www.R-project.org/`, ISBN 3-900051-07-0.

Railsback, S. F., Grimm, V., 2011. Agent-Based and Individual-Based Modeling: A Practical Introduction. Princeton University Press, Princeton.

Reppas, A. I., Tsoumanis, A. C., Siettos, C. I., 2010. Coarse-grained bifurcation analysis and detection of criticalities of an individual-based epidemiological network model with infection control. Appl. Math. Model. 34 (3), 552–560.

Scheffer, M., Bascompte, J., Brock, W. A., Brovkin, V., Carpenter, S. R., Dakos, V., Held, H., van Nes, E. H., Rietkerk, M., Sugihara, G., 2009. Early-warning signals for critical transitions. Nature 461 (7260), 53–59.

Schneider, S. H., Dickinson, R. E., 1974. Climate modeling. Rev. Geophys. Space Phys. 12, 447–493.

Scholl, H. J., 2001. Agent-based and system dynamics modeling: A call for cross study and joint research. In: Proceedings of the 34th Annual Hawaii International Conference on System Sciences. Vol. 3. Manui, Hawaii.

Schouten, J. C., Takens, F., van den Bleek, C. M., 1994. Maximum-likelihood estimation of the entropy of an attractor. Phys. Rev. E 49 (1), 126–129.

Siekmann, I., Mar. 2015. Bifurcation analysis of individual-based models in population dynamics. Ecol. Complex. 21.

Siettos, C. I., Gear, C. W., Kevrekidis, I. G., 2012. An equation-free approach to agent-based computation: Bifurcation analysis and control of stationary states. Europhys. Lett. 99 (4), 48007.

Valladares, F., Matesanz, S., Guilhaumon, F., Araújo, M. B., Balaguer, L., Benito-Garzón, M., Cornwell, W., Gianoli, E., van Kleunen, M., Naya, D. E., Nicotra, A. B., Poorter, H., Zavala, M. A., 2014. The effects of phenotypic plasticity and local adaptation on forecasts of species range shifts under climate change. Ecol. Lett. 17 (11), 1351–1364.

van Baalen, M., 2000. Pair approximations for different spatial geometries. In: Dieckmann, U., Law, R., Metz, J. A. (Eds.), The Geometry of Ecological Interactions: Simplifying Spatial Complexity. Cambridge University Press, Cambridge, pp. 359–387.

van Voorn, G. A. K., Hemerik, L., Boer, M. P., Kooi, B. W., 2007. Heteroclinic orbits indicate overexploitation in predator–prey systems with a strong Allee effect. Math. Biosci. 209 (2), 451–469.

Vautard, R., Ghil, M., 1989. Singular spectrum analysis in nonlinear dynamics, with applications to paleoclimatic time series. Physica D 35, 395–424.

Vautard, R., Yiou, P., Ghil, M., 1992. Singular spectrum analysis: A toolkit for short noisy chaotic signals. Physica D 58, 95–126.

Walker, B., Holling, C. S., Carpenter, S. R., Kinzig, A., 2004. Resilience, adaptability and transformability in social–ecological systems 9 (2), 5.

Wang, J., Shi, J., Wei, J., 2011. Predator–prey system with strong Allee effect in prey. J. Math. Biol. 62 (3), 291–331.

Wilenski, U., 1999. NetLogo. `http://ccl.northwestern.edu/netlogo/`.

Wissel, C., 1984. A universal law of the characteristic return time near thresholds. Oecologia 65 (1), 101–107.

Łomnicki, A., 1999. Individual-based models and the individual-based approach to population ecology. Ecol. Model. 115 (2-3), 191–198.